The Impacts of Biomass Burning Activities on Convective Systems in the Maritime Continent

Hsiang-He Lee[1*@] and Chien Wang[1,2**]

[1] Center for Environmental Sensing and Modeling, Singapore-MIT Alliance for Research and Technology, Singapore

[2] Center for Global Change Science, Massachusetts Institute of Technology, Cambridge, MA, U.S.A.

[*]Now at Atmospheric, Earth, and Energy Division, Lawrence Livermore National Laboratory, Livermore, CA, U.S.A.

[**]Now at Laboratoire d'Aerologie/CNRS/University of Toulouse, Toulouse, France

Submitted to

Atmospheric, Chemistry and Physics

July 2019

[@]Corresponding author address: Dr. Hsiang-He Lee, 7000 East Avenue, Livermore, CA, 94550, U.S.A.

E-mail: lee1061@llnl.gov

Abstract

Convective precipitation associated with Sumatra squall lines and diurnal rainfall over Borneo is an important weather feature of the Maritime Continent in Southeast Asia. Over the past few decades, biomass burning activities have been widespread during summertime over this region, producing massive fire aerosols. These additional aerosols brought to the atmosphere, besides influencing local radiation budget through directly scattering and absorbing sunlight, can also act as cloud condensation nuclei or ice nuclei to alter convective clouds and precipitation in the Maritime Continent via the so-called aerosol indirect effects. Based on four-month simulations with or without biomass burning aerosols conducted using the Weather Research and Forecasting model with chemistry package (WRF-Chem), we have investigated the aerosol-cloud interactions associated with the biomass burning aerosols in the Maritime Continent. Results from selected cases of convective events have shown significant impacts of fire aerosols specifically on the weak convections by increasing the quantities of hydrometeors and rainfall in both Sumatra and Borneo regions. Statistical analysis over the fire season also suggests that fire aerosols have impacts on the nocturnal convections associated with the local anticyclonic circulation in the western Borneo and then weakened the nocturnal rainfall intensity by about 9%. Such an effect is likely come from the near surface heating by absorbing aerosols emitted from fires that could weaken land breezes and thus the convergence of anticyclonic circulation.

1 Introduction

Biomass burning in Southeast Asia has become a serious environmental and societal issue in the past decade due to its impact on local economy, air quality, and public health (Miettinen et al., 2011; Kunii et al., 2002; Frankenberg et al., 2005; Crippa et al., 2016; Lee et al., 2018). Abundant aerosols emitted from such fires not only cause environmental issues but also affect regional weather and climate through the direct and indirect effects of biomass burning aerosols (Grandey et al., 2016; Hodzic and Duvel, 2017; Jeong and Wang, 2010; Ramanathan and Carmichael, 2008; Taylor, 2010; Tosca et al., 2013). Carbonaceous compounds such as black carbon (BC) in biomass burning aerosols can reduce sunlight through both absorption and scattering to warm the atmosphere while cool the Earth's surface (Fujii et al., 2014; Andreae and Gelencsér, 2006; Satheesh and Ramanathan, 2000; Ramanathan et al., 2001). Besides these direct effects, biomass burning aerosols can act as cloud condensation nuclei or ice nuclei to alter cloud microphysical structures and thus cloud radiation. Such "indirect effects" of these aerosols on the climate are even more complicated due to various cloud and meteorological conditions (Sekiguchi et al., 2003; Lin et al., 2013; Wu et al., 2013; Grandey et al., 2016; Ramanathan et al., 2001; Wang, 2004).

For the Maritime Continent in Southeast Asia, convective precipitation associated with the so-called Sumatra squall lines (SSL) and diurnal rainfall over Borneo is an important weather feature (Lo and Orton, 2016; Ichikawa and Yasunari, 2006; Koh and Teo, 2009; Yi and Lim, 2006; Wu et al., 2009). Convections of SSL are initially formed in the northwestern side of Sumatra by the prevailing sea breezes from Indian Ocean and the Sumatran mountain range, then propagate over the Malacca Strait affecting the Malay

79 Peninsula. Lo and Orton (2016) analyzed 22-year (1988 to 2009) ground-based Doppler
80 radar data and identified a total of 1337 squall lines in Singapore. They found that these
81 events with the diurnal cycle of rainfall most occur during either the summer monsoon
82 season (June-September) or the inter-monsoon periods (April-May and October-
83 November). Singapore, for example, experiences typically about 6~7 squall lines per
84 month during these periods. Oki and Musiake (1994) analyzed the seasonal and diurnal
85 cycles of precipitation using rain gauge data and showed that large-scale low-level winds
86 are a critical modulating factor in the diurnal cycle the convective rainfall over Borneo
87 besides the general reason of land-sea contrast behind convective rainfall in the Maritime
88 Continent. Furthermore, Ichikawa and Yasunari (2006) used five years Tropical Rainfall
89 Measuring Mission (TRMM) precipitation radar (PR) data to investigate the role of the
90 low-level prevailing wind in modulating the diurnal cycle of rainfall over Borneo. They
91 found that the diurnal cycle is associated with intraseasonal variability in the large-scale
92 circulation pattern, with regimes associated with either low-level easterlies or westerlies
93 over the island.

94 Interestingly, frequent biomass burning activities coincide with vigorous convective
95 systems in the Maritime Continent, especially during the summer monsoon season (June-
96 September), and could thus produce aerosols to affect convections in the region.
97 Rosenfeld (1999) analyzed TRMM data and hypothesized that abundant biomass burning
98 aerosols could practically shut off warm rain processes in tropical convective clouds.
99 Compared to the adjacent tropical clouds in the cleaner air, clouds encountered with
100 smokes could grow to higher altitudes with rain suppressed, hypothetically due to the
101 reduction of coalescence efficiency of smaller cloud drops into raindrops. Recently,

using Weather Research and Forecasting model with Chemistry (WRF-Chem), Ge et al. (2014) have studied the direct and semi-direct radiative effects of biomass burning aerosols over the Maritime Continent and found the radiative effect of biomass burning aerosols could alter planetary boundary layer (PBL) height, local winds (including sea breeze), and cloud cover. However, relative coarse resolution (27 km) adopted in their simulation would not be able to reveal more details about how biomass burning aerosols affect convective clouds through modifying cloud microphysics processes. Whereas, Hodzic and Duvel (2017) have conducted a 40-day simulation using WRF-Chem with a convection-permitting scale (4 km) to study the fire aerosol-convection interaction during boreal summer in 2009 near the central Borneo mountainous region. Their result suggests that modifications of the cloud microphysics by biomass burning aerosols could reduce shallow precipitation in the afternoon and lead to a warm PBL anomaly at sunset, all lead to an enforcement of deep convection at night. However, they have also indicated that the radiative processes of moderately absorbing aerosols tend to reduce deep convection over most regions due to local surface cooling and atmosphere warming that increase the static stability, hence suggesting the complexity of the interaction of biomass burning aerosols and convective clouds in the Maritime Continent.

In this study, we aim to examine and quantify the impacts of biomass burning aerosols on convective systems over two targeted regions for analyses: the northern Sumatra and the western Borneo in the Maritime Continent. Our focus is on not only the change of hydrometeors in the convective clouds but also the change of rainfall amount and intensity in these regions. We firstly describe methodologies adopted in the study, followed by the results and findings from our numerical simulations over the Maritime

Continent. We have selected three cases in each study region to perform detail analyses. In addition, statistical analyses covering the entire modeled fire season for each of these two regions have also been performed to provide more generalized pictures about the effects of fire aerosol on convection. The last section summarizes and concludes our work.

2 Methodology

2.1 Model and emission inventories

In order to simulate trace gases and particulates interactively with the meteorological fields, the Weather Research and Forecasting model coupled with a chemistry module (WRF-Chem, see Grell et al. (2005)) version 3.6.1 is used in this study. Within WRF-Chem, the Regional Acid Deposition Model, version 2 (RADM2) photochemical mechanism (Stockwell et al., 1997) coupled with the Modal Aerosol Dynamics Model for Europe (MADE) as well as the Secondary Organic Aerosol Model (SORGAM) (Ackermann et al., 1998; Schell et al., 2001) are included to simulate atmospheric chemistry and anthropogenic aerosol evolutions. MADE/SORGAM uses a modal approach to represent the aerosol size distribution and predicts mass and number concentrations of three aerosol modes (Aiken, accumulation, and coarse).

To resolve the convective system in the Maritime Continent in our simulations, two model domains with two-way nesting are designed. Here, Domain 1 (431 × 141 grid cells) has a resolution of 25 km, while Domain 2 (561 × 591 grid cells) has a resolution of 5 km (Fig. 1). Specifically, Domain 1 is positioned to include the tropical Indian Ocean on its west half in order to capture the path of Madden-Julian Oscillation (MJO),

147 and in the meantime to have a northern boundary constrained within 23°N in latitude to
148 avoid potential numerical instability from the terrain of Tibetan Plateau. Domain 2 with
149 a finer resolution is positioned to cover the mainland Southeast Asia as well as the islands
150 of Sumatra and Borneo.

151 The National Center for Environment Prediction FiNaL (NCEP-FNL) reanalysis
152 data (National Centers for Environmental Prediction, 2000) are used to provide initial and
153 boundary meteorological conditions, and to perform four-dimensional data assimilation
154 (FDDA) to nudge model temperature, water vapor, and zonal and meridional wind speeds
155 above the planetary boundary layer (PBL) for Domain 1. The time frequency of nudging
156 is every 6 hrs. The Mellor-Yamada-Nakanishi-Niino level 2.5 (MYNN) (Nakanishi and
157 Niino, 2009) is chosen as the scheme for planetary boundary layer in this study. Other
158 physics schemes adopted in the simulations include Morrison two-moment microphysics
159 scheme (Morrison et al., 2009), RRTMG longwave and shortwave radiation schemes
160 (Mlawer et al., 1997; Iacono et al., 2008), Unified Noah land-surface scheme (Tewari et
161 al., 2004), and Grell-Freitas ensemble cumulus scheme (Grell and Freitas, 2014) (for
162 Domain 1 only). Owing to the main purpose of this study to reveal fire aerosol-
163 convection interaction through modeling a large quantity of convective systems
164 continually over a relatively long period, and the computational resource available to us
165 as well, we have adopted a 5 km horizontal resolution which excluding cumulus
166 parameterization scheme. Previous studies have shown that WRF model with a similar
167 resolution without convection parameterization can still capture many critical
168 characteristics of deep convection (Wagner et al., 2018). Our model evaluation,

169 especially through the comparison of modeled results with sounding profiles, has
170 demonstrated the same.

171 WRF-Chem needs emissions for gaseous and particulate precursors to drive its
172 simulations. For this purpose, we have used the Regional Emission inventory in ASia
173 (REAS) version 2.1 (Kurokawa et al., 2013). REAS includes emissions of most primary
174 air pollutants and greenhouse gases, covering each month from 2000 to 2008. In
175 addition, the Fire INventory from U.S. National Center for Atmospheric Research
176 (NCAR) version 1.5 (FINNv1.5) (Wiedinmyer et al., 2011) is also used in the study to
177 provide biomass burning emissions. FINNv1.5 classifies burnings of extratropical forest,
178 tropical forest (including peatland), savanna, and grassland. Fire heat fluxes for four
179 different types of fire are prescribed in WRF-Chem to calculate the plume height (rf.
180 Table 1 in Freitas et al. (2007)). For peatland fire, we have set its heat flux as 4.4 kW m^{-2}
181 , which is the same as that of savanna burning and differs from that of the tropical forest
182 burning in 30 kW m^{-2}. The modified the plume rise algorithm in WRF-Chem to
183 specifically improve the representation of tropical peat fire has been described in Lee et
184 al. (2017). It is worth indicating that the heat flux from biomass burning is not
185 incorporated in thermodynamic equation of current WRF-Chem model. Note that the
186 current fire emission inventories could underestimate near surface fire aerosol
187 concentration by ignoring some of the characteristics of smoldering burning as well (Shi
188 et al., 2019).

189 The default chemical profiles of several species in the lateral boundary condition are
190 higher than their background concentrations in our study region and thus equivalent to
191 provide additional aerosol sources from boundaries. To prevent this, we have set NO,

192 NO_2, SO_2, and all primary aerosol levels to zero at the lateral boundaries of Domain 1.
193 We have also adjusted the ozone profile used for lateral boundary condition based on the
194 World Meteorological Organization (WMO) Global Atmosphere Watch (GAW) station
195 in Bukit Kototabang, Indonesia (Lee et al., 2019).

196 2.2 Numerical experiment design

197 Two numerical simulations, both included anthropogenic emissions (mainly fossil
198 fuel emissions) while either with and without the biomass burning emissions (labeled as
199 FFBB and FF, respectively), have been conducted to investigate the impacts of biomass
200 burning aerosols on convective systems in the Maritime Continent through both direct
201 and indirect effects. Our study focuses on the fire season from June to September of
202 2008. Therefore, the simulations start from 1 May of 2008 and last for five months. The
203 first month is used as a spin-up period. Among the years with available emission data,
204 both emission amount of biomass burning and total precipitation in 2008 approximate
205 their ensemble mean or represent an average condition (Fig. S1). Nevertheless,
206 interannual variation of biomass burning emissions alongside precipitation in the studies
207 regions do exist (Lee et al., 2017; Lee et al., 2018), and the influence of such variation on
208 the effects of fire aerosol on convection should be addressed in future studies.

209 2.3 Analysis methods

210 The primary target of this study is the convective systems associated with Sumatra
211 squall lines and diurnal rainfall over Borneo. Thus, our analyses mainly focus on the
212 convections over two specific regions: the Sumatra region (r1 in Fig. 1) and the Borneo
213 region (r2 in Fig. 1). The area coverage of the Sumatra region (r1) is from 97° to 103° E

214 in longitude and 0° to 6° N in latitude, while the area coverage of the Borneo region (r2)
215 is from 109° to 115° E in longitude and 1° S to 5° N in latitude.

216 To examine the impacts of fire aerosols on cloud formation and rainfall intensity as
217 well as amount, we have selected three convective systems each for the two focused
218 regions to perform an in-depth case study. We first trace the path of individual
219 convections and focus the analyses on the specific area of each of these convective
220 systems to identify the impacts of fire aerosols. Table 1 shows the selected cases in the
221 Sumatra region (r1) and the Borneo region (r2). The selected cases are chosen randomly
222 from different fire periods of the two study regions. We did not set any criteria initially
223 when we chose these cases. After we analyzed all cases, 3 mm $3hr^{-1}$ was set as the
224 threshold to distinguish weak and strong convections.

225 The consequent analyses are then focused on the fire-season-wise statistics of
226 convections for each study region. Table 2 and Fig. S2 show the fire periods in the two
227 study regions. There are total of 54 convective systems simulated during the fire periods
228 in the Sumatra region (r1) and 35 convective systems in the Borneo region (r2).

229 The statistical quantities used in this study follows Wang (2005) to estimate the
230 mean value over a specific region (e.g., r1 or r2). The cloud area mean quantities are
231 defined as a function of output time step (t) by the following equation:

232 $$\bar{c}^{area}(t) = \frac{1}{N(t)} \sum_{\substack{q > qmin \\ n > nmin}} c(x, y, z, t). \quad (1)$$

233 Here *c* is a given quantity (e.g., cloud water mass). Eq. (1) only applies to the grid points
234 where both the mass concentration *q* and number concentration *n* of a hydrometeor
235 exceed their given minima. The total number of these grid points at a given output time
236 step *t* is represented by *N(t)*. The cloud area mean quantities are used to present the

237 average quantities of a given variable at a given output time step. Note that the cloud
238 area mean quantities only apply to hydrometeors. For rainfall, the analyzed quantities are
239 spatial averages over a specific area of the convective system for case study or over the
240 entire study region for longer-term statistic estimate.

241 # 3 Results

242 ## 3.1 Model evaluation

243 ### 3.1.1 Precipitation

244 The satellite-retrieved precipitation of the Tropical Rainfall Measuring Mission
245 (TRMM) 3B42 3hrly (V7) dataset (Huffman et al., 2007) is used in this study to evaluate
246 simulated rainfall. Figure 2a and 2b show the Hovmöller plots of daily TRMM and
247 FFBB precipitation from 1 June 2008 to 30 September 2008, respectively. Compared to
248 the satellite-retrieved data, the model has captured all the major rainfall events in the two
249 analysis regions (Fig. 3). In addition, because of its higher spatial resolution than
250 TRMM, the model produces more light rain events. Nevertheless, as indicated in our
251 previous study (Lee et al., 2017), a wet bias of the model is evident and mainly comes
252 from water vapor nudging in data assimilation (FDDA). As a result, the daily average
253 rainfall in FFBB over the Sumatra region (r1) is 11.05±5.90 mm day^{-1} from 1 June 2008
254 to 30 September 2008, higher than that of 7.21±5.54 mm day^{-1} derived from TRMM
255 retrieval. The wet bias also exists in the modeling results in the Borneo region (r2),
256 where daily average rainfall there is 15.40±8.49 mm day^{-1} in FFBB and only 9.56±7.20
257 mm day^{-1} in TRMM. For the simulated rainfall in FFBB, the temporal correlation with
258 TRMM is 0.44 in the Sumatra region (r1) and 0.64 in the Borneo region (r2).

3.1.2 Aerosol optical depth (AOD)

Because of limited ground-based observational data of aerosols, we use Aerosol Optical Depth (AOD) from the level-3 Moderate Resolution Imaging Spectroradiometer (MODIS) gridded atmosphere monthly global joint product (MOD08_M3; http://dx.doi.org/10.5067/MODIS/MOD08_M3.061) to evaluate modeled aerosol spatial distribution and relative concentration. Figure 4a shows MODIS monthly AOD in Southeast Asia in September 2008. High AOD occurs in the southern part of Sumatra and the southwestern part of Borneo. Compared to the MODIS retrieval, the modeled AOD in FFBB has similar spatial distribution but a higher value (Fig. 4b). It is because a high spatiotemporal resolution in our simulation enables the model to capture episodic fire events better. In contrast, FF simulation produces much lower AOD values than those of MODIS and FFBB, thus suggesting biomass burning aerosols make a substantial fraction in atmospheric AOD during burning seasons.

3.1.3 Sounding profiles

We have used multiple weather sounding profiles measured in Bintulu Airport, Malaysia (113.03° E, 3.20° N), provided by University of Wyoming (http://weather.uwyo.edu/upperair/sounding.html). An example for detailed summary is a case at 12 UTC on 22 September 2008 (Fig. 5a). This sounding provides information of atmospheric state (e.g., vertical distributions of pressure, temperature, wind speed, wind direction, and humidity) coinciding with one of our selected case study (r2c3) of diurnal convective rainfall in Borneo. Compared to the observed sounding data, the FFBB simulation has produced similar temperature and wind profiles and well captured

281 the low-level and high-level wind speeds and wind directions (Fig. 5a versus 5b). It also
282 well predicts several key indexes of convection: temperature and pressure of the Lifted
283 Condensation Level (LCL) simulated in FFBB are 296.2 K and 955 hPa, respectively,
284 which are close to the values of 296.2 K in temperature and 960.7 hPa in pressure derived
285 from the observed sounding data. The model predicts 3049 J of Convective Available
286 Potential Energy (CAPE), while 2031 J of CAPE is estimated in the observed sounding
287 data. Besides this 22 September 2008 case, the model has also captured major features of
288 observed profiles for all the other cases selected in our analyses shown in Fig. S3~S7.

289 ### 3.1.4 Cloud vertical structure

290 The Cloud-Aerosol Lidar and Infrared Pathfinder Satellite Observation (CALIPSO)
291 provides information of the vertical structure of clouds on its path around the globe
292 (https://www-calipso.larc.nasa.gov/products/lidar/browse_images/production/), including
293 that of one of our cases (r2c3) of diurnal convective rainfall in Borneo on 22 September,
294 2008 (Fig. 6a). For this case, CALIPSO shows the vertical structure of a convective
295 system over Borneo along with high $PM_{2.5}$ concentration near the surface (yellowish
296 color near the surface), implying a potential impact of biomass burning aerosols on
297 convective clouds. It can be seen that the FFBB simulations well captures the vertical
298 structure of convective clouds as well as the near-surface aerosol layers, including their
299 vertical extension (Fig. 6c versus 6a). With the comparison of FF simulation, we are able
300 to identify the biomass burning origin of these aerosols near the surface. It is worth to
301 indicate that we have compared more than 50 modeled convections during the fire season
302 and within the simulation domains. However, the others captured by CALIPSO are

either not among the selected cases or are mostly out of our analyzed domains, so we did not have further discussion here.

3.2 Analyses of selected cases in two study regions

3.2.1 The Sumatra region (r1)

The three selected cases in r1 or the Sumatra region (r1c1, r1c2 and r1c3) all occurred in the afternoon (2 PM or 5 PM local time) and lasted less than 24 hours (Table 1). The sounding profile of three cases show quite similar to the environmental profiles (Fig. S3~S5). Most fire aerosols in this study region were initially emitted from the central and south Sumatra then transported along with southwesterly winds to encounter convections in the northern Sumatra. Compared to the result of FF, $PM_{2.5}$ concentration in FFBB can be 6~12 times higher in the Sumatra region (r1) in these selected cases (Fig. 7).

Aerosols from biomass burning in FFBB add 2~3 times more cloud droplet number concentration and 8~20% higher cloud water mass compared to the results in FF (Table 2). The mean radius of cloud droplets in FFBB is about 6~7 μm, clearly smaller than that in FF (10~11 μm). Smaller cloud droplet in FFBB reduces the efficiency of autoconversion, and further decreases rain water mass and raindrop number concentration. Hence, raindrop number concentration in FFBB is 40~50% lower than that in FF among our selected cases in r1 (Table 3). However, besides autoconversion, rain water mass is also affected by other microphysics processes. Larger raindrops combining with smaller cloud droplets in FFBB can enhance the efficiency of cloud droplet collection by rain and thus increase rain water mass but cause no change to the

number of raindrops, possibly compensating the decrease of rain water mass resulted from a lowered autoconversion. Overall, rain water mass decreases 15% in the case of r1c2 and 10% in the case of r1c3, respectively. Compared to the cases of r1c2 and r1c3, the case of r1c1 is a relatively weak convective system based on a threshold of ~3 mm $3hr^{-1}$ of the averaged rainfall in FF (Table 4). After introducing fire aerosols, the mass concentration of snow and graupel in this case increases 62% and 48%, respectively. Melting snow and graupel in the lower atmosphere results in a significant increase of rain water mass concentration by 49%. Thus, total hydrometeor mass is increased by 36% in FFBB from that in FF. Our result is consistent with that of Lin et al. (2006), which suggested that biomass burning aerosols could invigorate convection and then increase precipitation based on satellite observations. The aerosol invigoration effect is referred to such a hypothetic process that increasing number of smaller cloud droplets due to higher aerosol concentration would reduce the efficiency of raindrop formation from self-collection among cloud droplets, and thus further slowdown the loss of these small droplets from being collected by larger raindrops and allow more of them reach high altitudes, where they would eventually collected by ice particles through riming, causing release of latent heat to enhance updraft (Rosenfeld et al., 2008). For tropical regions with high humidity, additional aerosols may also lead to the warm-phase invigoration due to the consequent enhancement in total condensed water quantity and thus latent heat release (Wang, 2005; Fan et al., 2018). Note that the "aerosol-aware" microphysics scheme in WRF-Chem only applies to the warm cloud process (Morrison et al., 2005; Morrison et al., 2009); therefore, ice nucleation is parameterized of ambiance temperature only regardless of the aerosol concentration. In our model configuration, fire aerosol can

still affect ice process, however, through CCN effect rather than serving directly as ice nuclei.

In the FF simulations, the convective system in the case of r1c2 and r1c3 is stronger than the system in the case of r1c1, and the average rainfall of r1c2 and r1c3 is also higher than the rainfall of r1c1 (Table 4). Adding fire aerosols in FFBB does not substantially change the average rainfall in r1c2 and r1c3 (+3% and -8%, respectively; Table 4). However, in the relatively weak convective system of r1c1, adding fire aerosols significantly increases the mean rainfall amount by 106% (1.33±0.47 mm $3hr^{-1}$ in FF versus 2.74±1.21 mm $3hr^{-1}$ in FFBB).

3.2.2 The Borneo region (r2)

The three selected cases in r2 (r2c1, r2c2, and r2c3) also occurred during the summer monsoon season when active biomass burning events existed in the west Borneo. In these cases, fire aerosols were transported to the north and northeast by the southeasterly and southwesterly winds. Because of the proximity of fire emissions, the $PM_{2.5}$ concentration in FFBB can be 24 times higher than that in FF in the Borneo region (r2) in these selected cases (Fig. 7).

The modeled results demonstrate the substantial impacts of fire aerosols on both ambient aerosol concentration and cloud droplet number concentration. $PM_{2.5}$ concentration in FFBB is drastically higher than that in FF with the highest increase appears in the case of r2c1 at 4940%, more than doubled the values of r2c2 (2402%) and r2c3 (2422%). The increase in cloud droplet number concentration in the case of r2c1 (703%) is also substantially higher than those in r2c2 (337%) and r2c3 (409%) (Table 2).

370 The mean radius of cloud droplets in FFBB is about 6~7 μm, which is significantly
371 smaller than that in FF (10~11 μm). The mean cloud droplet radii in FF and FFBB in r2
372 are similar to the results in r1. On the other hand, the increase of cloud water mass due to
373 fire aerosols is not so dramatic in all these cases, only about 8%~27% higher than that in
374 the FF simulations (Table 3). As discussed above, rain number concentration in FFBB
375 over the Borneo region (r2) is lower than that in FF, similar to the cases in r1, likely due
376 to the low efficiency of autoconversion induced by the presence of a large quantity of
377 smaller cloud droplets. Rain water mass of FFBB in the r2c1 case is decreased by about
378 6% due to fire aerosols, which is similar to the results in the r1c2 and r1c3 cases over the
379 Sumatra region (Table 3). However, interestingly, rain water and snow mass are both
380 increased in FFBB by 64% and 69% in r2c2 and by 19% and 60% in r2c3, respectively
381 (Table 3). The cases of r2c2 and r2c3 are relatively weak convective systems, similar to
382 the case of r1c1. Again, it is based on based on a threshold of ~3 mm $3hr^{-1}$ of the
383 averaged rainfall in FF (Table 4). Our results show that fire aerosols have substantial
384 impacts on cold cloud processes in the weak convective systems. Overall, total
385 hydrometeor mass concentration in FFBB have increased 47% in r2c2 and 13% in r2c3.

386 The changes of rainfall amount due to fire aerosols in r2 are similar to the cases in r1.
387 For the strong convection case of r2c1, adding fire aerosols in the FFBB simulation
388 decreases the total rainfall amount by 18%. However, in the weak convection cases of
389 r2c2 and r2c3, adding fire aerosols would double the rainfall amount (Table 4).
390 Compared to the results in FF, rainfall intensity is persistently higher in FFBB during the
391 convection life cycle in those weak convection cases. Nighttime rainfall intensity in
392 FFBB, especially, is much higher than the rainfall intensity in FF. Therefore, as shown

by our results, fire aerosols appear to have more substantial impacts on the quantities of hydrometeors and rainfall of the weak convection cases in both Sumatra region (r1) and Borneo region (r2).

Our results show that fire aerosols tend to invigorate weak convection but suppress deep convection in both Sumatra region (r1) and Borneo region (r2). As mentioned before, increasing the number of smaller cloud droplets due to higher aerosol concentration resulted from fire would reduce the efficiency of raindrop formation through the warm-rain processes, thus allowing more cloud droplets reach high altitudes to be eventually collected by ice particles through riming, causing release of latent heat to invigorate updraft while enhancing precipitation through melting of fallen ice particles (Wang, 2005). These processes appear to be more effective to weak convections than deep convections and were in fact well-simulated in the former cases. The results are also consistent with some previous observation-based studies (Jiang et al., 2018; Zhao et al., 2018). Jiang et al. (2018) and Zhao et al. (2018) both concluded that an increase of fire aerosols generally reduces cloud optical thickness of deep convection while Zhao et al. (2018) further showed that fire aerosols tend to invigorate weak convection for small-to-moderate aerosol loadings.

3.3 Fire-season statistics of convections in two study regions

Statistics covering the entire simulated fire season (~4 months) for each study region have been derived to provide trend/tendency information regarding several aspects of the impact of fire aerosols on convections. In our simulations, $PM_{2.5}$ concentration in FF during the fire periods, which can be regarded as the background value for FFBB

415 simulation before adding fire aerosols, is 1.36±0.19 μg m^{-3} in r1 and 0.56±0.09 μg m^{-3} in
416 r2. In comparison, $PM_{2.5}$ concentration in FFBB is 11.37±10.41 μg m^{-3} in r1 and
417 10.07±7.73 μg m^{-3} in r2. Note that unlike in some other studies where the control
418 simulations use constant aerosol concentrations, fire aerosol concentrations in our
419 simulations can vary in responses to changes in fire emissions, or aerosol removal by rain
420 scavenging due to precipitation change caused by fire aerosols themselves. Hence, the
421 processes included in our simulations are closer to reality, and the results could better
422 reflect the nature of fire aerosol-convection interaction in the Maritime Continent.

423 Averaged through the entire modeled fire periods, cloud water mass (Qc), cloud
424 droplet number concentration (Qnc), and rain drop number concentration (Qnr) in FFBB
425 differ substantially from those in FF, demonstrating the influence of fire aerosols. Figure
426 8 shows that adding fire aerosols in FFBB would increase Qc by 14% and Qnc by 226%
427 in r1, and Qc by 18% and Qnc by 349% in r2. Another pronounced change in response to
428 adding fire aerosols is a decrease in Qnr by 44% in r1 and 47% in r2. Although an
429 increase in snow mass (Qs) and graupel mass (Qg) and a decrease in rain water mass (Qr)
430 after adding fire aerosols, the uncertainty of these hydrometeor changes is large.

431 In Sect. 3.2, we have discussed the significant rainfall increase occurred in the weak
432 convective systems after adding fire aerosols due to aerosol invigoration effect. On one
433 hand, regardless the strength of convection, the mean 3-hourly rainfall during the fire
434 periods is 1.06±0.85 mm in FF and 1.09±0.86 mm in FFBB over the Sumatra region (r1),
435 and statistically it does not change significantly in responding to fire aerosols. The
436 rainfall difference in the Borneo region (r2) between FF and FFBB is also insignificant
437 (1.32±1.20 mm $3hrs^{-1}$ in FF versus 1.35±1.14 mm $3hrs^{-1}$ in FFBB). On the other hand,

438 we have found that the impacts of fire aerosols appear in several other rainfall patterns.
439 For instance, the daily maximum and minimum rainfalls display clear differences
440 between the FFBB and FF simulations, specifically in r2 rather than in r1 (Fig. 9). While
441 for r1, the impacts of fire aerosol are reflected in event-wise statistics, e.g., higher event-
442 wise maximum and minimum rainfall intensity in FFBB than in FF, identified in 30 out
443 of 54 convective events in total. These are mostly weak convective events in r1.
444 Interestingly, somewhat opposite to the rainfall statistics in r1, the intensity of event-wise
445 maximum and minimum rainfall in r2 is higher in FF than in FFBB. The daily rainfall
446 peak of 3-hr rainfall in r1 is mostly less than 3 mm; in comparison, one-third of
447 convective events in r2 have daily maximum 3-hr rainfall exceeding 3 mm (Fig. 9c),
448 suggesting that the convective systems in r2 tend to develop stronger than in r1 and the
449 fire aerosols significantly suppress the maximum rainfall intensity of strong convections
450 in r1. We roughly used 1.25 mm $3hr^{-1}$ of the domain-averaged rainfall to classify weak
451 and strong convective systems. We find that the conclusions regarding differences of
452 hydrometers and rainfall in the weak systems between the FF and FFBB experiments stay
453 the same, and such differences are still not that significant in both regions (Table S1 and
454 Fig. S8).

455 We have categorized the maximum rainfall based on its values in the afternoon and
456 midnight. We find that those heavy maximum rainfalls in r2 tend to occur in the
457 midnight (Fig. 9c) associated with the anticyclonic circulation formed in the western
458 Borneo induced by southeasterly winds from the Southern latitude turn northeastward
459 along the west coast of Borneo, owing to the terrain of Borneo Island and the sea breezes
460 from the South China Sea. The vortex produced by such a circulation leads to strong

updraft and then strong convection. Note that this anticyclonic circulation is different from the Borneo vortex, the latter appears as a persistent feature of the boreal winter climatology and is related to the northeasterly from the South China Sea and cold surge events (Chang et al., 1983; Chang et al., 2005).

The low-level wind pattern of Borneo convections is similar to the westerly regime, especially the weak westerly (WW) regime identified by Ichikawa and Yasunari (2006). According to their analysis, the WW regime tends to occur in boreal summer. Its composites include an anticyclonic feature with the weak wind field over the Borneo Island. The deep convective storms developed in the WW regime tend to stay close to the west coast associated with the lower-level convergence enhanced by the prevailing wind and local circulations around there, resulting in localized rainfall over the offshore region of the west coast. Based on our simulations, the onset of convection occurs in the afternoon over the western mountain range of Borneo. These storms would consequently evolve into widespread shallow storms in the evening over the western part of the island. The maximum rainfall appears on the west coast because of a local westward propagating rainfall system that develops around midnight or early morning.

The comparison of the maximum rainfall between FF and FFBB in Fig. 9 shows that fire aerosols tend to reduce the maximum rainfall, especially for high-intensity rainfall events. In other words, fire aerosols have substantial impacts on the nocturnal convections, which are associated with the local anticyclonic circulation in the western Borneo. This effect on nocturnal convections in the western Borneo by fire aerosols will be discussed further in the next section.

3.4 The impact of biomass burning aerosols on nocturnal convections in the Borneo region

To further analyze the effects of fire aerosols on nocturnal convections, we have categorized convective events into nocturnal convections (NC) and non-nocturnal convections (non-NC), based on whether the maximum rainfall occurs from midnight to early morning or in the time frame from late afternoon to evening. Figure 10 shows the diurnal time series of precipitation averaged over the Borneo region (r2) in FF and FFBB. Again, 3-hour-mean rainfalls of nocturnal convections are higher than those of non-nocturnal convections in both simulations and fire aerosols weaken the maximum nocturnal rainfall intensity about 9%.

Nocturnal convections tend to stay close to the west coast associated with a lower-level convergence enhanced by the prevailing wind and local circulations mainly related to the land breezes from inland of the western Borneo. The strong convergence near the surface over the offshore region of the west coast causes the weak westerly monsoon windflaws and local land breezes to merge during the nighttime. However, during the fire periods, the daytime absorption of fire aerosols (e.g., black carbon) can cause an atmospheric warming (even without fire generated heating flux being incorporated in the model). This could increase near surface air temperature, weaken land breezes and thus surface convergence. As a result, the nocturnal convections in FFBB cannot develop as strong as those in FF. On the other hand, both nocturnal and non-nocturnal convections are initiated over the western mountain range under a prevailing wind of the sea breezes from the South China Sea. The increases of near surface temperature owing to the fire

505 aerosols can enhance this prevailing wind from the ocean and thus lead to a higher
506 convective rainfall in FFBB during the onset stage of the nocturnal convections as well as
507 non-nocturnal convections. Figure 11 illustrates the sea breeze increase in FFBB during
508 the daytime (20 LST) and the land breeze decrease in FFBB during the nighttime (2
509 LST). Twenty LST and 2 LST are chosen here because of the peak of difference.

510 Diurnal evolution of vertical profiles clearly indicates that mass mixing ratio of total
511 hydrometeors, temperature, and vertical velocity differ in both daytime and nighttime
512 between FF and FFBB for those nocturnal convections (Fig. 12). The differences of near
513 surface temperature between FF and FFBB are more pronounced during the period after
514 sunset (Fig. 12d). The differences of near surface temperature mainly happen over land,
515 and the higher near surface temperature in FFBB weakens the land breezes and near
516 surface convergence along the coast. Starting from late afternoon, (about 5 PM local
517 time), vertical velocity increases with time until sunrise next day in both simulations (Fig.
518 12e) due to the convergence of the monsoon windflaws and local land breezes during the
519 nighttime, and this matches very well with that of mass mixing ratio of total
520 hydrometeors (Fig. 12a and 12e). Noticeably, the main differences in vertical velocity
521 and hydrometeor mass mixing ratio between FFBB and FF also start to become evident
522 after entering the evening. Because of the weaker convergence near the surface in FFBB,
523 the differences in vertical velocity at the higher altitude between FFBB and FF peaks in
524 the nighttime. The temperature increase from aerosol absorption seems small (please
525 note that the direct heating from fire is not included in the WRF fire plume model) but we
526 do see the change of vertical velocity owing to the aerosol heating effect. Based on our
527 analysis, the temperature increase is mainly associated with the thermodynamic

perturbation from the absorption of sunlight by fire aerosols. This seems also consistent with the analysis of Zhang et al. (2019). Indeed, should the heat flux generated by fires be incorporated in the model, the warming effects from biomass burning would be much stronger and also persist in nocturnal timeframe.

As a summary, the schematics shown in Fig. 13 illustrate the impact of biomass burning activities on nocturnal convections in the Borneo region. In the daytime, under the prevailing wind of sea breezes from the South China Sea, convections develop over the western mountain range. Because near surface heating from the absorption of sunlight by fire aerosols could enhance the prevailing wind from the ocean, convective rainfall becomes higher at the onset stage of the nocturnal convections (still in daytime) due to biomass burning activities (Fig. 13b). In the nighttime, convection moves to the offshore region of the western Borneo. The strong convergences near the surface merge the weak westerly monsoon windflaws with local nighttime land breezes to form an anticyclonic circulation (Fig. 13c). During the fire periods, the daytime near surface warming by fire aerosols could also further weaken land breezes and surface convergence. Hence, the nocturnal convections during fire events would not develop as strong as in days without fires (Fig. 13d versus 13c).

4 Summary

By comparing WRF-Chem modeling results include or exclude biomass burning emissions (FFBB versus FF), we have identified certain detailed impacts of fire aerosols on convective events within two study regions in the Maritime Continent during a four-month period (June 2008 ~ September 2008). In total, 54 convective systems in the

550 Sumatra region and 35 convective systems in the Borneo region have been simulated.
551 Three convective events of each study region have been selected for in-depth
552 investigation. In addition, statistical analyses have been performed throughout the entire
553 simulation period for each region. We have focused our analyses on two rainfall
554 features: 1) convective precipitation associated with Sumatra squall lines, and 2) diurnal
555 rainfall over the western Borneo.

556 We find that fire aerosols lead to the increase of cloud water mass and cloud droplet
557 number concentration among all analyzed cases while a substantial reduction of rain drop
558 number concentration. Influences of fire aerosols on other hydrometeors vary from case
559 to case. Specifically, our results show that fire aerosols can significantly change the
560 quantities of hydrometeors, particularly those involved in cold cloud processes and
561 rainfall of weak convections in either the Sumatra region or the Borneo region. Rainfall
562 intensity is higher in FFBB during the entire convection life cycle in those weak
563 convection cases, and the nighttime rainfall intensity in FFBB is significantly higher than
564 that in FF.

565 Statistics performed throughout the entire modeled fire season shows that the fire
566 aerosols only cause a nearly negligible change (2-3%) to the total rainfall of convective
567 systems in both study regions. On the other hand, we notice that fire aerosols can still
568 alter daily maximum and minimum rainfall in some cases, for example, fire aerosols lead
569 to the increase of maximum and minimum rainfall intensity in 30 weak convective events
570 in the Sumatra region.

571 In the Borneo region, biomass burning activities mainly affect the rainfall intensity
572 of nocturnal convection. Because near surface heating from the absorption of fire

aerosols can enhance the prevailing wind from the ocean (sea breeze) during the daytime, the convective rainfall over the western mountain range is higher during the onset stage of the nocturnal convections. In the nighttime, the consequence of the above thermodynamic perturbation by absorbing fire aerosols can further weaken land breeze and surface convergence. Hence, the rainfall intensity of nocturnal convections under the influence of fire aerosols would become weaker by about 9%.

This study has demonstrated how biomass burning activities could affect convective systems in the Maritime Continent by altering cloud microphysics and dynamics. We find the biomass burning activities significantly change the diurnal rainfall intensity, especially those low-level wind patterns associated with the weak westerly (WW) regime as suggested by Ichikawa and Yasunari (2006). Our results show that neither a single case study nor a simple statistical summary applied to overall model simulation period without in-depth analyses could reveal the impact of biomass burning aerosols on convections under different windflaw regimes.

Data availability

FINNv1.5 emission data are publicly available from http://bai.acom.uar.edu/Data/fire/. REAS emission data can be downloaded from https://www.nies.go.jp/REAS/. TRMM data can be obtained from https://pmm.nasa.gov/data-access/downloads/trmm. AOD from MODIS can be obtained from http://dx.doi.org/10.5067/MODIS/MOD08_M3.061. Sounding profiles are publicly available on http://weather.uwyo.edu/upperair/sounding.html. WRF-Chem simulated data are available upon request from Hsiang-He Lee (lee1061@llnl.gov).

Author contribution

H.-H. L. and C. W. designed the experiments and H.-H. L. carried them out. H.-H. L. configured the simulations and analyzed the results. H.-H. L. and C. W. wrote the manuscript.

Declaration of Competing Interest

The authors declare that they have no known competing financial interests or personal relationships that could have appeared to influence the work reported in this paper.

Acknowledgments

This research was supported by the National Research Foundation Singapore through the Singapore-MIT Alliance for Research and Technology, the interdisciplinary research program of Center for Environmental Sensing and Modeling. It was also supported by the U.S. National Science Foundation (AGS-1339264) and L'Agence National de la Recherche (ANR) of France under the "Programme d'Investissements d'Avenir", ANR-18-MPGA-003 EUROACE. The authors would like to acknowledge NCEP-FNL and NCAR FINN working groups for releasing their data to the research communities; and the NCAR WRF developing team for providing the numerical model for this study. The computational work for this article was performed on resources of the National Supercomputing Centre, Singapore (https://www.nscc.sg).

Reference:

Ackermann, I. J., Hass, H., Memmesheimer, M., Ebel, A., Binkowski, F. S., and Shankar, U.: Modal aerosol dynamics model for Europe: development and first applications, Atmospheric Environment, 32, 2981-2999, http://dx.doi.org/10.1016/S1352-2310(98)00006-5, 1998.

Andreae, M. O., and Gelencsér, A.: Black carbon or brown carbon? The nature of light-absorbing carbonaceous aerosols, Atmos. Chem. Phys., 6, 3131-3148, 10.5194/acp-6-3131-2006, 2006.

Chang, C.-P., Millard, J. E., and Chen, G. T. J.: Gravitational Character of Cold Surges during Winter MONEX, Monthly Weather Review, 111, 293-307, 10.1175/1520-0493(1983)111<0293:gcocsd>2.0.co;2, 1983.

Chang, C.-P., Harr, P. A., and Chen, H.-J.: Synoptic Disturbances over the Equatorial South China Sea and Western Maritime Continent during Boreal Winter, Monthly Weather Review, 133, 489-503, 10.1175/mwr-2868.1, 2005.

Crippa, P., Castruccio, S., Archer-Nicholls, S., Lebron, G. B., Kuwata, M., Thota, A., Sumin, S., Butt, E., Wiedinmyer, C., and Spracklen, D. V.: Population exposure to hazardous air quality due to the 2015 fires in Equatorial Asia, Scientific Reports, 6, 37074, 10.1038/srep37074, 2016.

Fan, J., Rosenfeld, D., Zhang, Y., Giangrande, S. E., Li, Z., Machado, L. A. T., Martin, S. T., Yang, Y., Wang, J., Artaxo, P., Barbosa, H. M. J., Braga, R. C., Comstock, J. M., Feng, Z., Gao, W., Gomes, H. B., Mei, F., Pöhlker, C., Pöhlker, M. L., Pöschl, U., and de Souza, R. A. F.: Substantial convection and precipitation enhancements by ultrafine aerosol particles, Science, 359, 411-418, 10.1126/science.aan8461, 2018.

Frankenberg, E., McKee, D., and Thomas, D.: Health consequences of forest fires in Indonesia, Demography, 42, 109-129, 10.1353/dem.2005.0004, 2005.

Freitas, S. R., Longo, K. M., Chatfield, R., Latham, D., Silva Dias, M. A. F., Andreae, M. O., Prins, E., Santos, J. C., Gielow, R., and Carvalho Jr, J. A.: Including the sub-grid scale plume rise of vegetation fires in low resolution atmospheric transport models, Atmos. Chem. Phys., 7, 3385-3398, 10.5194/acp-7-3385-2007, 2007.

Fujii, Y., Iriana, W., Oda, M., Puriwigati, A., Tohno, S., Lestari, P., Mizohata, A., and Huboyo, H. S.: Characteristics of carbonaceous aerosols emitted from peatland fire in Riau, Sumatra, Indonesia, Atmospheric Environment, 87, 164-169, http://dx.doi.org/10.1016/j.atmosenv.2014.01.037, 2014.

Ge, C., Wang, J., and Reid, J. S.: Mesoscale modeling of smoke transport over the Southeast Asian Maritime Continent: coupling of smoke direct radiative effect below and above the low-level clouds, Atmos. Chem. Phys., 14, 159-174, 10.5194/acp-14-159-2014, 2014.

Grandey, B. S., Lee, H. H., and Wang, C.: Radiative effects of interannually varying vs. interannually invariant aerosol emissions from fires, Atmos. Chem. Phys., 16, 14495-14513, 10.5194/acp-16-14495-2016, 2016.

Grell, G. A., Peckham, S. E., Schmitz, R., McKeen, S. A., Frost, G., Skamarock, W. C., and Eder, B.: Fully coupled "online" chemistry within the WRF model, Atmospheric Environment, 39, 6957-6975, 10.1016/j.atmosenv.2005.04.027, 2005.

659 Grell, G. A., and Freitas, S. R.: A scale and aerosol aware stochastic convective
660 parameterization for weather and air quality modeling, Atmos. Chem. Phys., 14,
661 5233-5250, 10.5194/acp-14-5233-2014, 2014.
662 Hodzic, A., and Duvel, J. P.: Impact of Biomass Burning Aerosols on the Diurnal
663 Cycle of Convective Clouds and Precipitation Over a Tropical Island, Journal of
664 Geophysical Research: Atmospheres, 123, 1017-1036, 10.1002/2017JD027521,
665 2017.
666 Huffman, G. J., Bolvin, D. T., Nelkin, E. J., Wolff, D. B., Adler, R. F., Gu, G., Hong, Y.,
667 Bowman, K. P., and Stocker, E. F.: The TRMM Multisatellite Precipitation Analysis
668 (TMPA): Quasi-Global, Multiyear, Combined-Sensor Precipitation Estimates at Fine
669 Scales, Journal of Hydrometeorology, 8, 38-55, 10.1175/JHM560.1, 2007.
670 Iacono, M. J., Delamere, J. S., Mlawer, E. J., Shephard, M. W., Clough, S. A., and
671 Collins, W. D.: Radiative forcing by long-lived greenhouse gases: Calculations with
672 the AER radiative transfer models, Journal of Geophysical Research: Atmospheres,
673 113, 10.1029/2008JD009944, 2008.
674 Ichikawa, H., and Yasunari, T.: Time–Space Characteristics of Diurnal Rainfall
675 over Borneo and Surrounding Oceans as Observed by TRMM-PR, Journal of Climate,
676 19, 1238-1260, 10.1175/jcli3714.1, 2006.
677 Jeong, G. R., and Wang, C.: Climate effects of seasonally varying Biomass Burning
678 emitted Carbonaceous Aerosols (BBCA), Atmos. Chem. Phys., 10, 8373-8389,
679 10.5194/acp-10-8373-2010, 2010.
680 Jiang, J. H., Su, H., Huang, L., Wang, Y., Massie, S., Zhao, B., Omar, A., and Wang, Z.:
681 Contrasting effects on deep convective clouds by different types of aerosols, Nature
682 Communications, 9, 3874, 10.1038/s41467-018-06280-4, 2018.
683 Koh, T.-Y., and Teo, C.-K.: TOWARD A MESOSCALE OBSERVATION NETWORK IN
684 SOUTHEAST ASIA, Bulletin of the American Meteorological Society, 90, 481-488,
685 10.1175/2008bams2561.1, 2009.
686 Kunii, O., Kanagawa, S., Yajima, I., Hisamatsu, Y., Yamamura, S., Amagai, T., and
687 Ismail, I. T. S.: The 1997 Haze Disaster in Indonesia: Its Air Quality and Health
688 Effects, Archives of Environmental Health: An International Journal, 57, 16-22,
689 10.1080/00039890209602912, 2002.
690 Kurokawa, J., Ohara, T., Morikawa, T., Hanayama, S., Janssens-Maenhout, G.,
691 Fukui, T., Kawashima, K., and Akimoto, H.: Emissions of air pollutants and
692 greenhouse gases over Asian regions during 2000–2008: Regional Emission
693 inventory in ASia (REAS) version 2, Atmos. Chem. Phys., 13, 11019-11058,
694 10.5194/acp-13-11019-2013, 2013.
695 Lee, H.-H., Bar-Or, R. Z., and Wang, C.: Biomass burning aerosols and the low-
696 visibility events in Southeast Asia, Atmos. Chem. Phys., 17, 965-980, 10.5194/acp-
697 17-965-2017, 2017.
698 Lee, H.-H., Iraqui, O., Gu, Y., Yim, S. H. L., Chulakadabba, A., Tonks, A. Y. M., Yang,
699 Z., and Wang, C.: Impacts of air pollutants from fire and non-fire emissions on the
700 regional air quality in Southeast Asia, Atmos. Chem. Phys., 18, 6141-6156,
701 10.5194/acp-18-6141-2018, 2018.
702 Lee, H.-H., Iraqui, O., and Wang, C.: The Impact of Future Fuel Consumption on
703 Regional Air Quality in Southeast Asia, Scientific Reports, 9, 2648, 10.1038/s41598-
704 019-39131-3, 2019.

Lin, J. C., Matsui, T., Pielke Sr., R. A., and Kummerow, C.: Effects of biomass-burning-derived aerosols on precipitation and clouds in the Amazon Basin: a satellite-based empirical study, Journal of Geophysical Research: Atmospheres, 111, 10.1029/2005jd006884, 2006.

Lin, N.-H., Tsay, S.-C., Maring, H. B., Yen, M.-C., Sheu, G.-R., Wang, S.-H., Chi, K. H., Chuang, M.-T., Ou-Yang, C.-F., Fu, J. S., Reid, J. S., Lee, C.-T., Wang, L.-C., Wang, J.-L., Hsu, C. N., Sayer, A. M., Holben, B. N., Chu, Y.-C., Nguyen, X. A., Sopajaree, K., Chen, S.-J., Cheng, M.-T., Tsuang, B.-J., Tsai, C.-J., Peng, C.-M., Schnell, R. C., Conway, T., Chang, C.-T., Lin, K.-S., Tsai, Y. I., Lee, W.-J., Chang, S.-C., Liu, J.-J., Chiang, W.-L., Huang, S.-J., Lin, T.-H., and Liu, G.-R.: An overview of regional experiments on biomass burning aerosols and related pollutants in Southeast Asia: From BASE-ASIA and the Dongsha Experiment to 7-SEAS, Atmospheric Environment, 78, 1-19, http://dx.doi.org/10.1016/j.atmosenv.2013.04.066, 2013.

Lo, J. C. F., and Orton, T.: The general features of tropical Sumatra Squalls, Weather, 71, 175-178, 10.1002/wea.2748, 2016.

Miettinen, J., Shi, C., and Liew, S. C.: Deforestation rates in insular Southeast Asia between 2000 and 2010, Global Change Biology, 17, 2261-2270, 10.1111/j.1365-2486.2011.02398.x, 2011.

Mlawer, E. J., Taubman, S. J., Brown, P. D., Iacono, M. J., and Clough, S. A.: Radiative transfer for inhomogeneous atmospheres: RRTM, a validated correlated-k model for the longwave, Journal of Geophysical Research: Atmospheres, 102, 16663-16682, 10.1029/97JD00237, 1997.

Morrison, H., Curry, J. A., and Khvorostyanov, V. I.: A New Double-Moment Microphysics Parameterization for Application in Cloud and Climate Models. Part I: Description, Journal of the Atmospheric Sciences, 62, 1665-1677, 10.1175/jas3446.1, 2005.

Morrison, H., Thompson, G., and Tatarskii, V.: Impact of Cloud Microphysics on the Development of Trailing Stratiform Precipitation in a Simulated Squall Line: Comparison of One- and Two-Moment Schemes, Monthly Weather Review, 137, 991-1007, 10.1175/2008mwr2556.1, 2009.

Nakanishi, M., and Niino, H.: Development of an Improved Turbulence Closure Model for the Atmospheric Boundary Layer, Journal of the Meteorological Society of Japan. Ser. II, 87, 895-912, 10.2151/jmsj.87.895, 2009.

National Centers for Environmental Prediction, N. W. S. N. U. S. D. o. C.: NCEP FNL Operational Model Global Tropospheric Analyses, continuing from July 1999, 10.5065/D6M043C6, 2000.

Oki, T., and Musiake, K.: Seasonal Change of the Diurnal Cycle of Precipitation over Japan and Malaysia, Journal of Applied Meteorology, 33, 1445-1463, 10.1175/1520-0450(1994)033<1445:scotdc>2.0.co;2, 1994.

Ramanathan, V., Crutzen, P. J., Lelieveld, J., Mitra, A. P., Althausen, D., Anderson, J., Andreae, M. O., Cantrell, W., Cass, G. R., Chung, C. E., Clarke, A. D., Coakley, J. A., Collins, W. D., Conant, W. C., Dulac, F., Heintzenberg, J., Heymsfield, A. J., Holben, B., Howell, S., Hudson, J., Jayaraman, A., Kiehl, J. T., Krishnamurti, T. N., Lubin, D., McFarquhar, G., Novakov, T., Ogren, J. A., Podgorny, I. A., Prather, K., Priestley, K., Prospero, J. M., Quinn, P. K., Rajeev, K., Rasch, P., Rupert, S., Sadourny, R., Satheesh, S. K., Shaw, G. E., Sheridan, P., and Valero, F. P. J.: Indian Ocean Experiment: An

751 integrated analysis of the climate forcing and effects of the great Indo-Asian haze,
752 Journal of Geophysical Research: Atmospheres, 106, 28371-28398,
753 10.1029/2001jd900133, 2001.
754 Ramanathan, V., and Carmichael, G.: Global and regional climate changes due to
755 black carbon, Nature Geosci, 1, 221-227, 2008.
756 Rosenfeld, D.: TRMM observed first direct evidence of smoke from forest fires
757 inhibiting rainfall, Geophysical Research Letters, 26, 3105-3108,
758 10.1029/1999gl006066, 1999.
759 Rosenfeld, D., Lohmann, U., Raga, G. B., O'Dowd, C. D., Kulmala, M., Fuzzi, S.,
760 Reissell, A., and Andreae, M. O.: Flood or Drought: How Do Aerosols Affect
761 Precipitation?, Science, 321, 1309-1313, 10.1126/science.1160606, 2008.
762 Satheesh, S. K., and Ramanathan, V.: Large differences in tropical aerosol forcing
763 at the top of the atmosphere and Earth's surface, Nature, 405, 60-63,
764 10.1038/35011039, 2000.
765 Schell, B., Ackermann, I. J., Hass, H., Binkowski, F. S., and Ebel, A.: Modeling the
766 formation of secondary organic aerosol within a comprehensive air quality model
767 system, Journal of Geophysical Research: Atmospheres (1984–2012), 106, 28275-
768 28293, 2001.
769 Sekiguchi, M., Nakajima, T., Suzuki, K., Kawamoto, K., Higurashi, A., Rosenfeld, D.,
770 Sano, I., and Mukai, S.: A study of the direct and indirect effects of aerosols using
771 global satellite data sets of aerosol and cloud parameters, Journal of Geophysical
772 Research: Atmospheres, 108, 4699, 10.1029/2002JD003359, 2003.
773 Shi, H., Jiang, Z., Zhao, B., Li, Z., Chen, Y., Gu, Y., Jiang, J. H., Lee, M., Liou, K.-N., Neu,
774 J. L., Payne, V. H., Su, H., Wang, Y., Witek, M., and Worden, J.: Modeling Study of the
775 Air Quality Impact of Record-Breaking Southern California Wildfires in December
776 2017, Journal of Geophysical Research: Atmospheres, 124, 6554-6570,
777 10.1029/2019jd030472, 2019.
778 Stockwell, W. R., Kirchner, F., Kuhn, M., and Seefeld, S.: A new mechanism for
779 regional atmospheric chemistry modeling, Journal of Geophysical Research:
780 Atmospheres, 102, 25847-25879, 10.1029/97JD00849, 1997.
781 Taylor, D.: Biomass burning, humans and climate change in Southeast Asia,
782 Biodivers Conserv, 19, 1025-1042, 10.1007/s10531-009-9756-6, 2010.
783 Tewari, M., F. Chen, W. Wang, J. Dudhia, M. A. LeMone, K. Mitchell, M. Ek, G.
784 Gayno, J. Wegiel, and Cuenca, R. H.: Implementation and verification of the unified
785 NOAH land surface model in the WRF model, 20th conference on weather analysis
786 and forecasting/16th conference on numerical weather prediction, Seattle, WA,
787 U.S.A., 2004.
788 Tosca, M. G., Randerson, J. T., and Zender, C. S.: Global impact of smoke aerosols
789 from landscape fires on climate and the Hadley circulation, Atmos. Chem. Phys., 13,
790 5227-5241, 10.5194/acp-13-5227-2013, 2013.
791 Wagner, A., Heinzeller, D., Wagner, S., Rummler, T., and Kunstmann, H.: Explicit
792 Convection and Scale-Aware Cumulus Parameterizations: High-Resolution
793 Simulations over Areas of Different Topography in Germany, Monthly Weather
794 Review, 146, 1925-1944, 10.1175/mwr-d-17-0238.1, 2018.

795 Wang, C.: A modeling study on the climate impacts of black carbon aerosols,
796 Journal of Geophysical Research: Atmospheres, 109, n/a-n/a,
797 10.1029/2003JD004084, 2004.
798 Wang, C.: A modeling study of the response of tropical deep convection to the
799 increase of cloud condensation nuclei concentration: 1. Dynamics and microphysics,
800 Journal of Geophysical Research: Atmospheres, 110, D21211,
801 10.1029/2004JD005720, 2005.
802 Wiedinmyer, C., Akagi, S. K., Yokelson, R. J., Emmons, L. K., Al-Saadi, J. A., Orlando,
803 J. J., and Soja, A. J.: The Fire INventory from NCAR (FINN): a high resolution global
804 model to estimate the emissions from open burning, Geosci. Model Dev., 4, 625-641,
805 10.5194/gmd-4-625-2011, 2011.
806 Wu, P., Hara, M., Hamada, J.-i., Yamanaka, M. D., and Kimura, F.: Why a Large
807 Amount of Rain Falls over the Sea in the Vicinity of Western Sumatra Island during
808 Nighttime, Journal of Applied Meteorology and Climatology, 48, 1345-1361,
809 10.1175/2009jamc2052.1, 2009.
810 Wu, R., Wen, Z., and He, Z.: ENSO Contribution to Aerosol Variations over the
811 Maritime Continent and the Western North Pacific during 2000–10, Journal of
812 Climate, 26, 6541-6560, 10.1175/JCLI-D-12-00253.1, 2013.
813 Yi, L., and Lim, H.: Semi-Idealized COAMPS®* Simulations of Sumatra Squall
814 Lines: the Role of Boundary Forcing, in: Advances in Geosciences, 111-124, 2006.
815 Zhang, Y., Fan, J., Logan, T., Li, Z., and Homeyer, C. R.: Wildfire impact on
816 environmental thermodynamics and severe convective storms, Geophysical
817 Research Letters, 0, 10.1029/2019gl084534, 2019.
818 Zhao, B., Gu, Y., Liou, K.-N., Wang, Y., Liu, X., Huang, L., Jiang, J. H., and Su, H.:
819 Type-Dependent Responses of Ice Cloud Properties to Aerosols From Satellite
820 Retrievals, Geophysical Research Letters, 45, 3297-3306, 10.1002/2018gl077261,
821 2018.

822

823

824 Table 1. The case period of the selected cases in the Sumatra region (r1) and the Borneo
825 region (r2)

Case name	Case period
r1c1	2008/08/10 0900 UTC ~ 2008/08/11 0300 UTC
r1c2	2008/08/19 0600 UTC ~ 2008/08/20 0000 UTC
r1c3	2008/09/23 0900 UTC ~ 2008/09/24 0000 UTC
r2c1	2008/08/05 0900 UTC ~ 2008/08/06 0300 UTC
r2c2	2008/09/17 0600 UTC ~ 2008/09/17 2100 UTC
r2c3	2008/09/22 0300 UTC ~ 2008/09/23 0000 UTC

826
827
828

829 Table 2. The fire periods in the two study regions

The Sumatra region (r1)	The Borneo region (r2)
6/10/2008 ~ 6/20/2008	6/21/2008 ~ 6/27/2008
6/25/2008 ~ 6/28/2008	8/1/2008 ~ 8/8/2008
7/4/2008 ~ 7/7/2008	9/10/2008 ~ 9/30/2008
7/27/2008 ~ 8/20/2008	
9/17/2008 ~ 9/27/2008	

830
831

Table 3. The mean differences in percentage of FFBB to FF (i.e. (FFBB-FF)/FF × 100%) for each selected case over the main convection area in the Sumatra region (r1) and the Borneo region (r2). Qc, Qi, Qr, Qs and Qg represents cloud, ice, rain, snow, and graupel mass concentration respectively. Qnc, Qni, Qnr, Qns and Qng means number concentration for each hydrometeor.

Case	Qc	Qi	Qr	Qs	Qg	Qnc	Qni	Qnr	Qns	Qng
r1c1	8%	27%	49%	62%	48%	248%	55%	-41%	33%	39%
r1c2	20%	-6%	-15%	-25%	1%	349%	-1%	-45%	-11%	-6%
r1c3	18%	10%	-10%	3%	5%	311%	4%	-50%	11%	-6%
r2c1	27%	1%	-6%	-5%	-4%	703%	3%	-59%	4%	-5%
r2c2	22%	10%	64%	69%	58%	337%	24%	-32%	17%	57%
r3c3	8%	10%	19%	60%	-2%	409%	-5%	-66%	8%	-12%

838 Table 4. The averaged precipitation (mm $3hrs^{-1}$) of FFBB and FF for each selected case
839 over the main convection area in the Sumatra region (r1) and the Borneo region (r2).
840 Parentheses in the third column show the difference in percentage of FFBB to FF (i.e.
841 (FFBB-FF)/FF × 100%).
842

Case	FF	FFBB
r1c1	1.33±0.47	2.74±1.21 (+106%)
r1c2	2.97±1.42	3.05±1.49 (+3%)
r1c3	4.32±1.84	3.98±2.18 (-8%)
r2c1	3.73±2.64	3.07±1.21 (-18%)
r2c2	1.88±0.53	3.97±1.47 (+111%)
r3c3	0.54±0.53	1.10±1.02 (+103%)

843
844

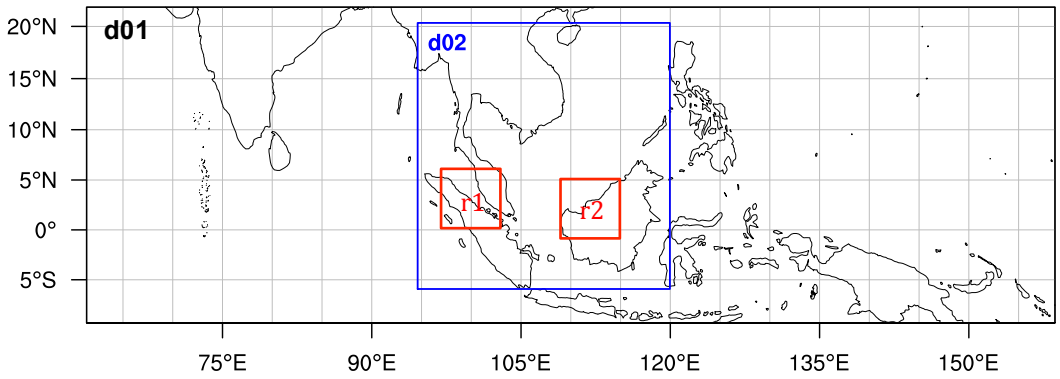

Figure 1. Domain configuration for WRF-Chem simulations. Domain 1 (d01) has a resolution of 25 km, while Domain 2 (d02) has a resolution of 5 km. Two red boxes indicate the two study regions: the Sumatra region (r1) and the Borneo region (r2).

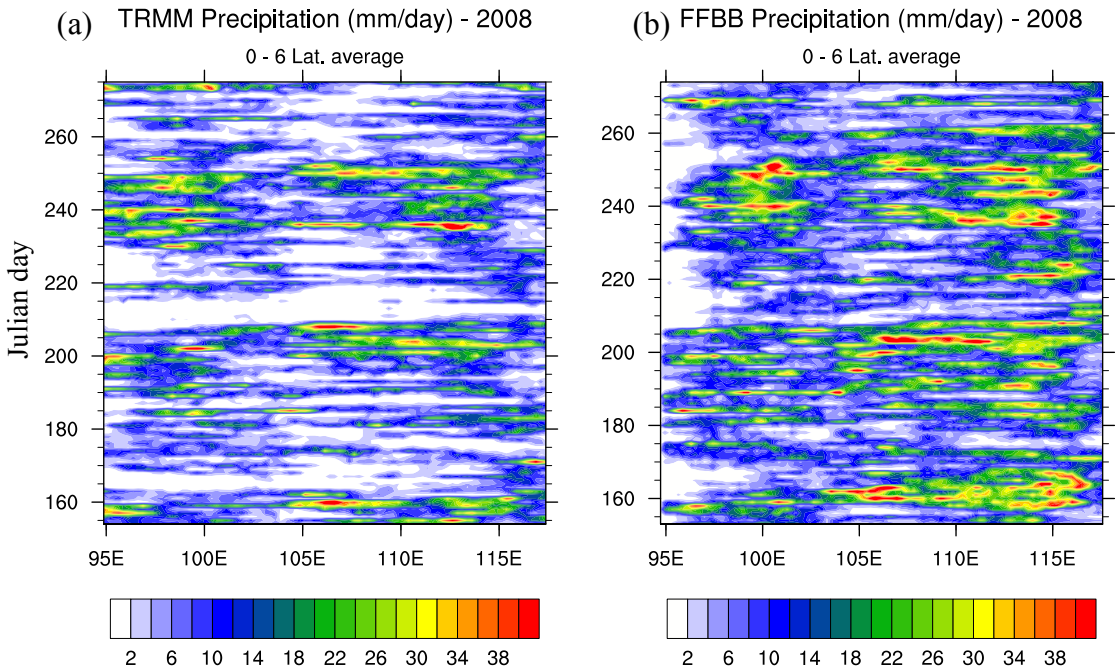

852
853 Figure 2. Hovmöller (time versus longitude) plot of daily precipitation (mm day^{-1}) from 1
854 June 2008 to 30 September 2008 from:(a) Tropical Rainfall Measuring Mission (TRMM)
855 and (b) FFBB. Latitude average is from 0° to 6°N.
856

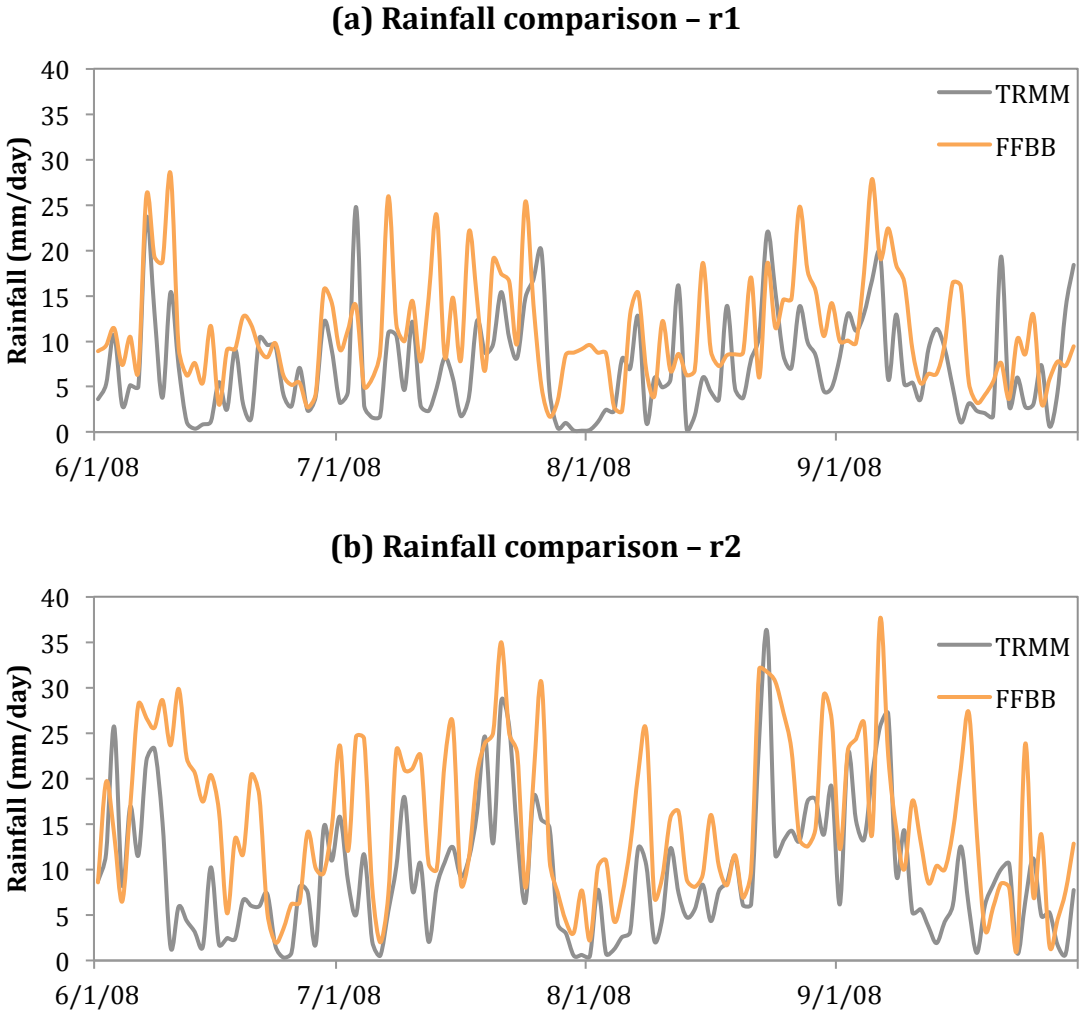

Figure 3. Time series of area-averaged daily rainfall (mm day^{-1}) from Tropical Rainfall Measuring Mission (TRMM) and FFBB over (a) the Sumatra region (r1) and (b) the Borneo region (r2).

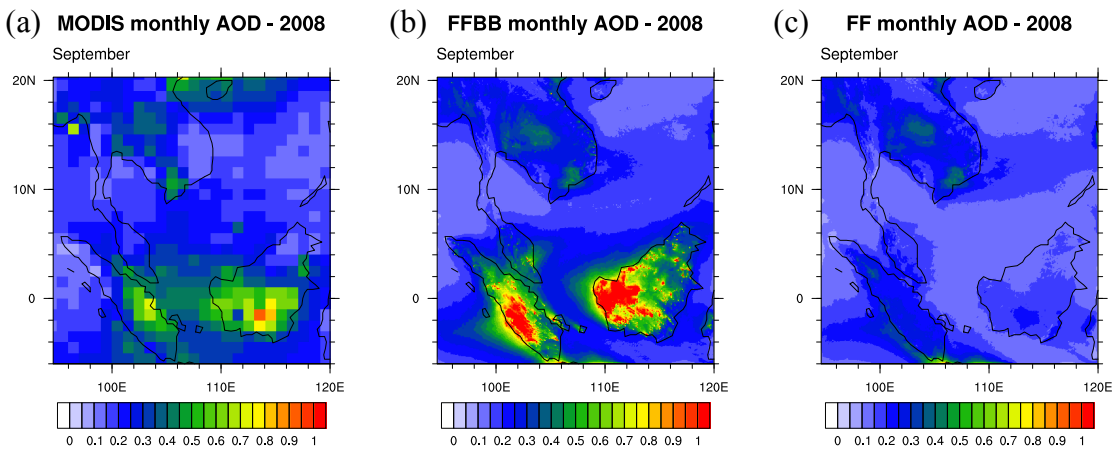

Figure 4. Monthly aerosol optical depth (AOD) in September 2008 from (a) Moderate Resolution Imaging Spectroradiometer (MODIS), (b) FFBB, and (c) FF.

(a)

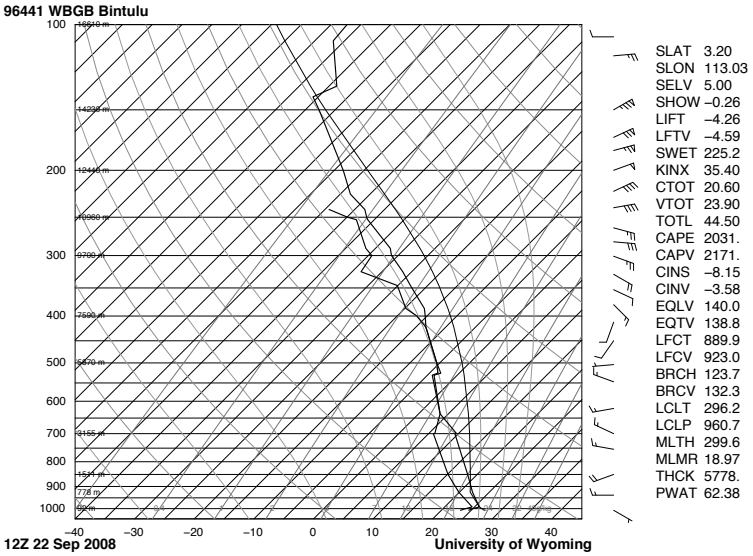

(b)

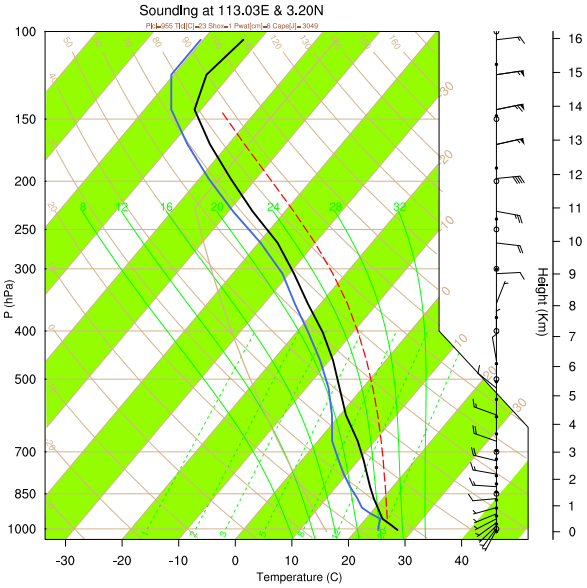

Figure 5. (a) Sounding profile observed at Bintulu Airport, Malaysia (113.03° E, 3.20° N) at 12 UTC on 22 September 2008. (b) Modeled sounding profile in FFBB at the same location and time as (a).

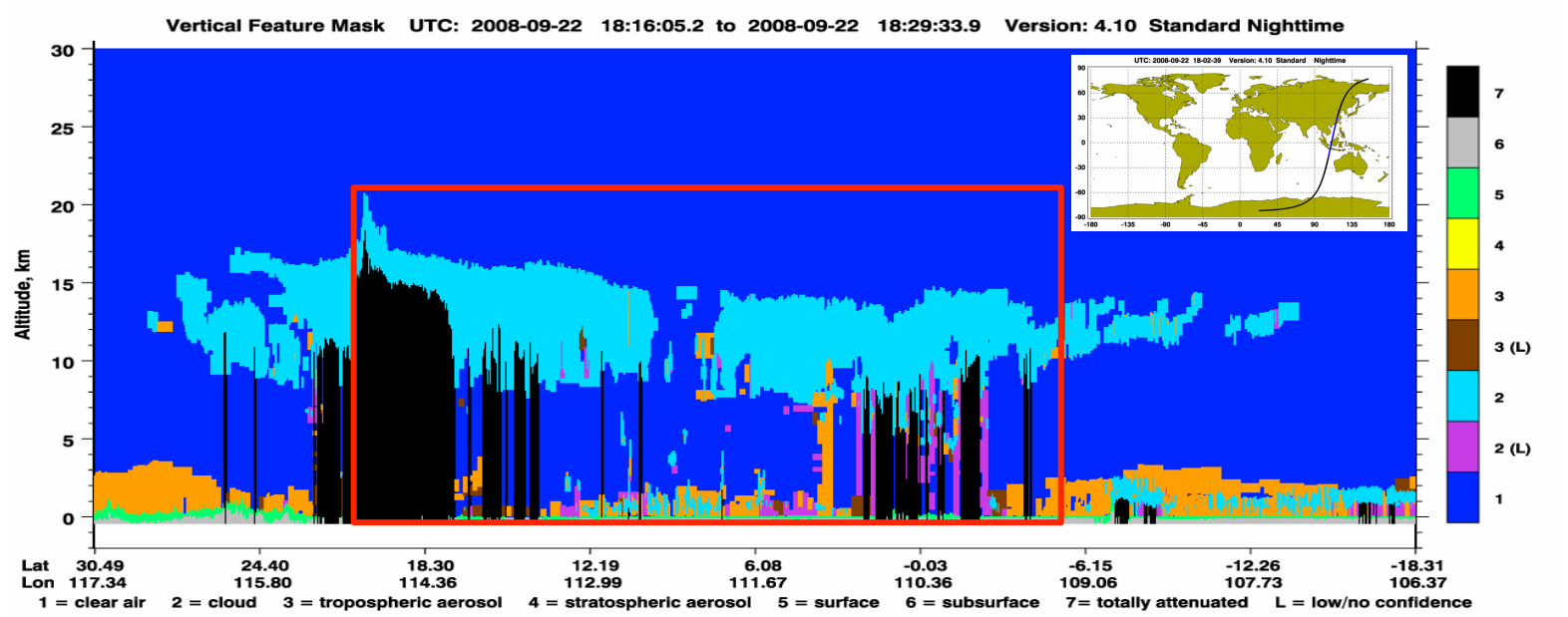

873
874
875

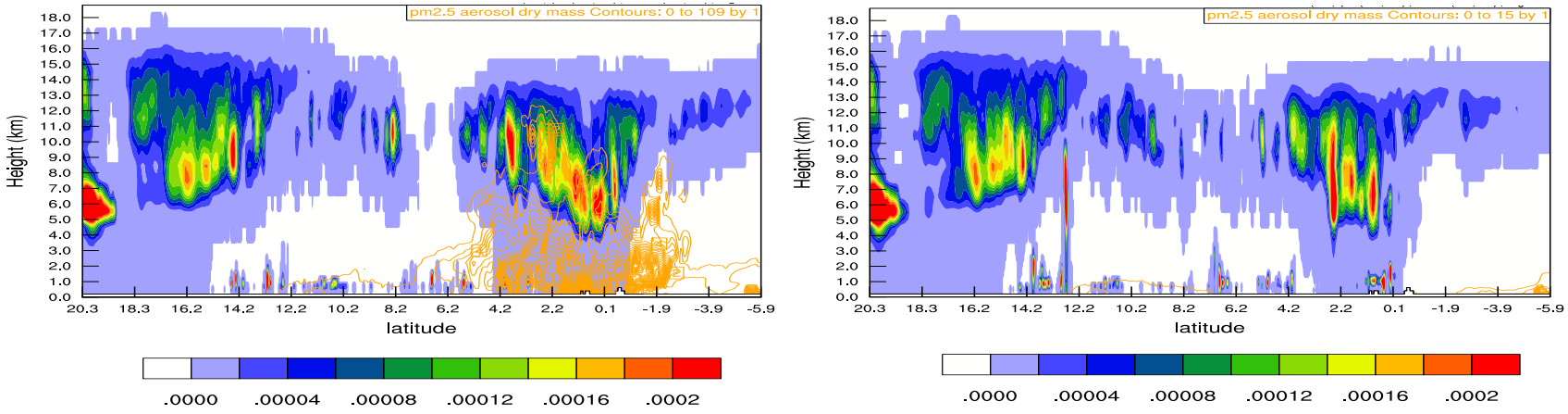

876

Figure 6 (a) The vertical structure of cloud retrieved from the Cloud-Aerosol Lidar and Infrared Pathfinder Satellite Observation (CALIPSO) on September 22, 2008. (b)-(c) The sum of simulated hydrometeor mixing ratio (shaded; kg kg^{-1}) and $PM_{2.5}$ concentration (contour; μg m^{-3}) in FFBB and FF, respectively. The profile domain of (b) and (c) is corresponding to the red rectangle in (a).

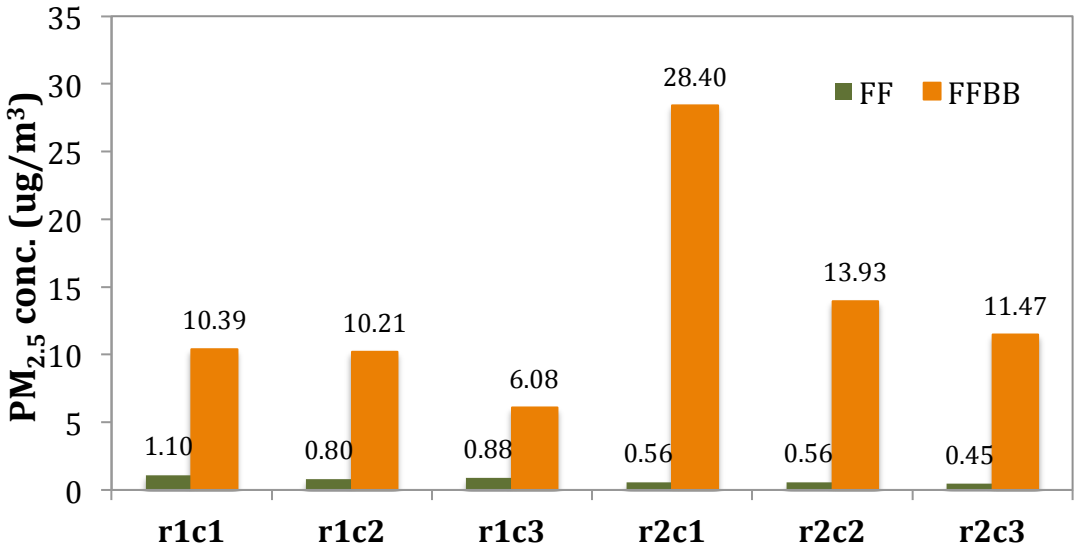

Figure 7. The mean $PM_{2.5}$ concentration (μg m^{-3}) in FF and FFBB for selected cases in the Sumatra region (r1) and the Borneo region (r2).

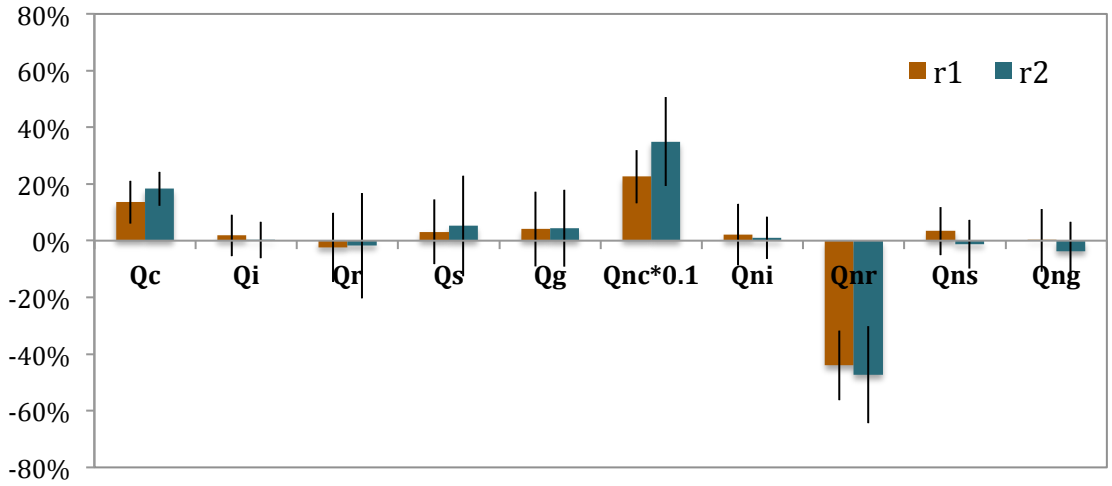

Figure 8. The mean differences in percentage of FFBB to FF (i.e. (FFBB-FF)/FF × 100%) over all convective cases during the fire periods in the Sumatra region (r1) and the Borneo region (r2). Qc, Qi, Qr, Qs and Qg represents cloud, ice, rain, snow, and graupel mass concentration, respectively. Qnc, Qni, Qnr, Qns and Qng means number concentration for each hydrometeor. The error bars represent one standard deviation.

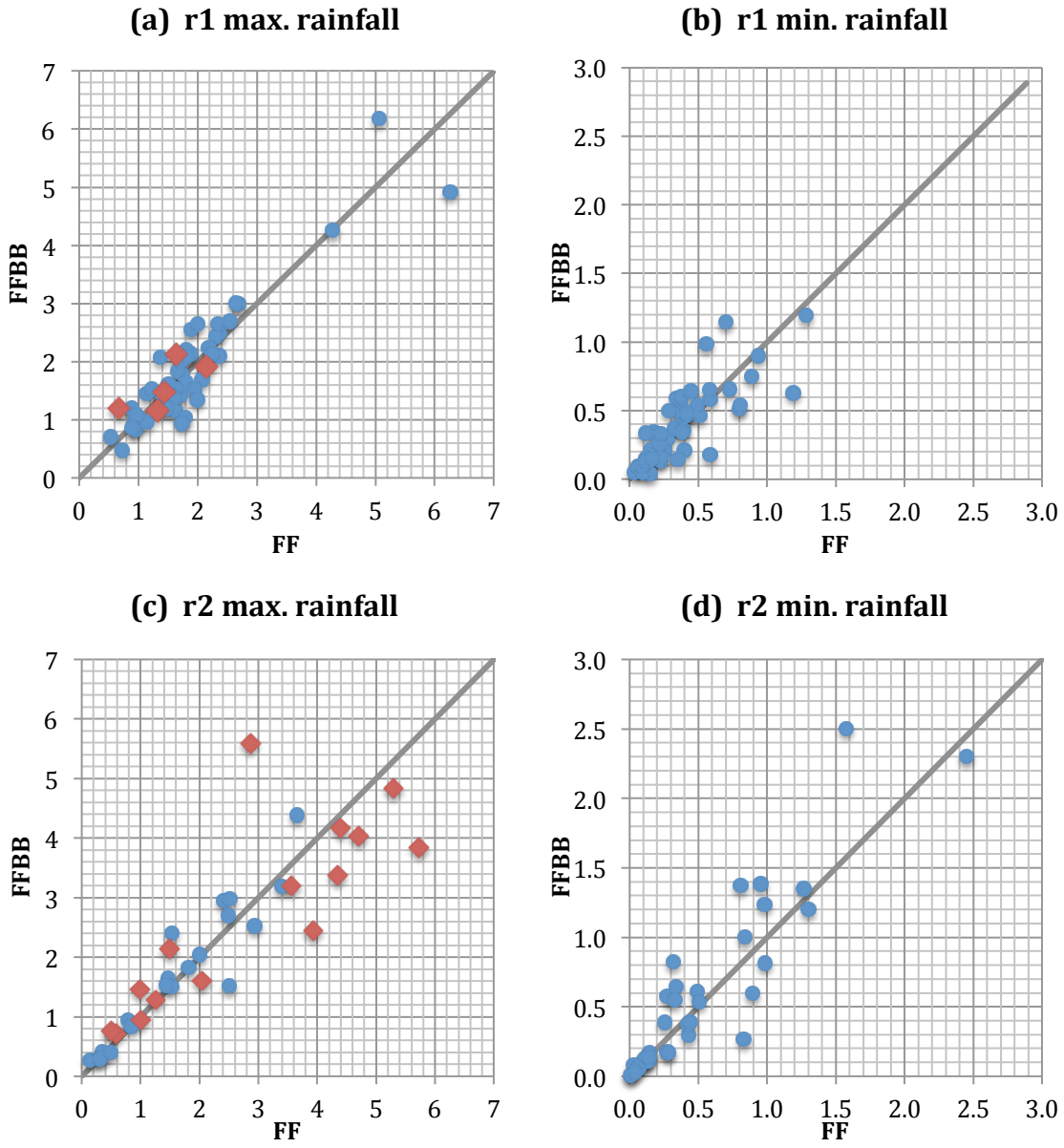

Figure 9. The scatterplots of daily maximum and minimum convective rainfall (mm $3hr^{-1}$) during the fire periods in in the Sumatra region (r1) and the Borneo region (r2). Red diamonds in (a) and (c) indicate that the maximum convective rainfall conducts in the midnight or early morning.

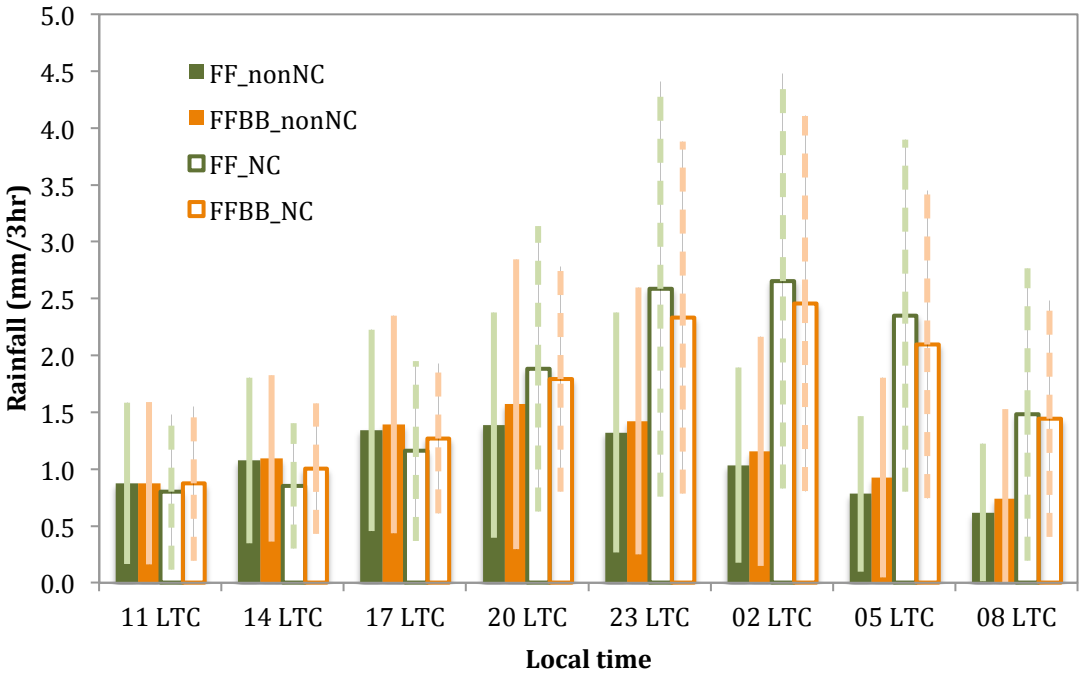

902
903 Figure 10. The diurnal time series of rainfall averaged over the Borneo region (r2) for
904 nocturnal convections (NC) and non- nocturnal convections (non-NC) during fire periods in
905 FF and FFBB. The error bars denote the standard deviation of the rainfall.
906
907

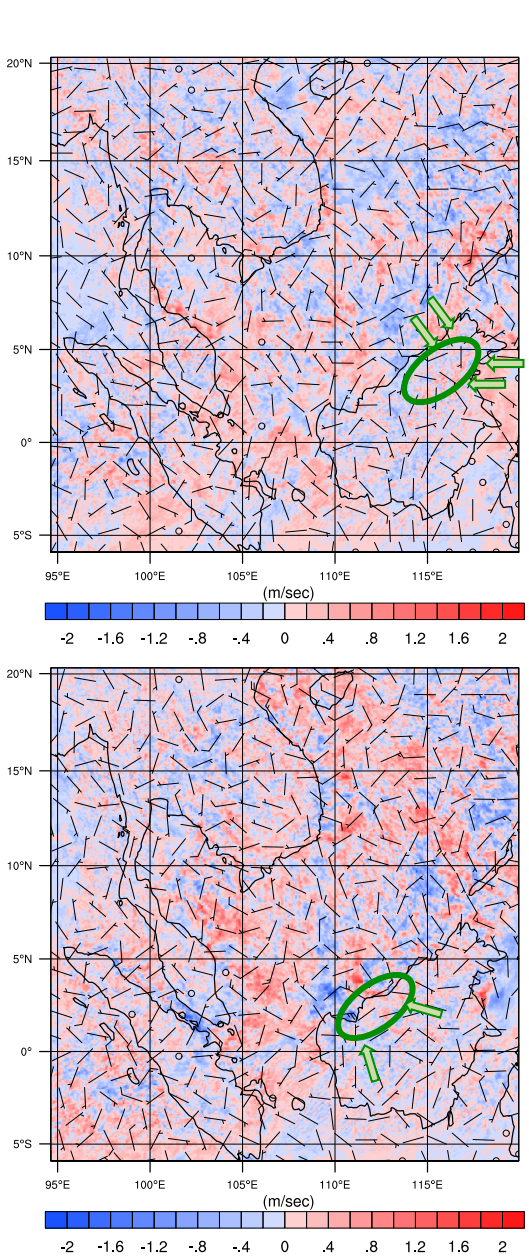

Figure 11. The mean wind field differences of FFBB and FF (FFBB-FF) at (a) 20 LST for non-nocturnal cases and (b) 02 LST for nocturnal cases in the Borneo region (r2). The green circle indicates the location of convections occurred. The green arrows mean the mean flow of sea breeze in (a) and land breeze in (b). The magnitude of wind barbs is 10 times higher than the real value.

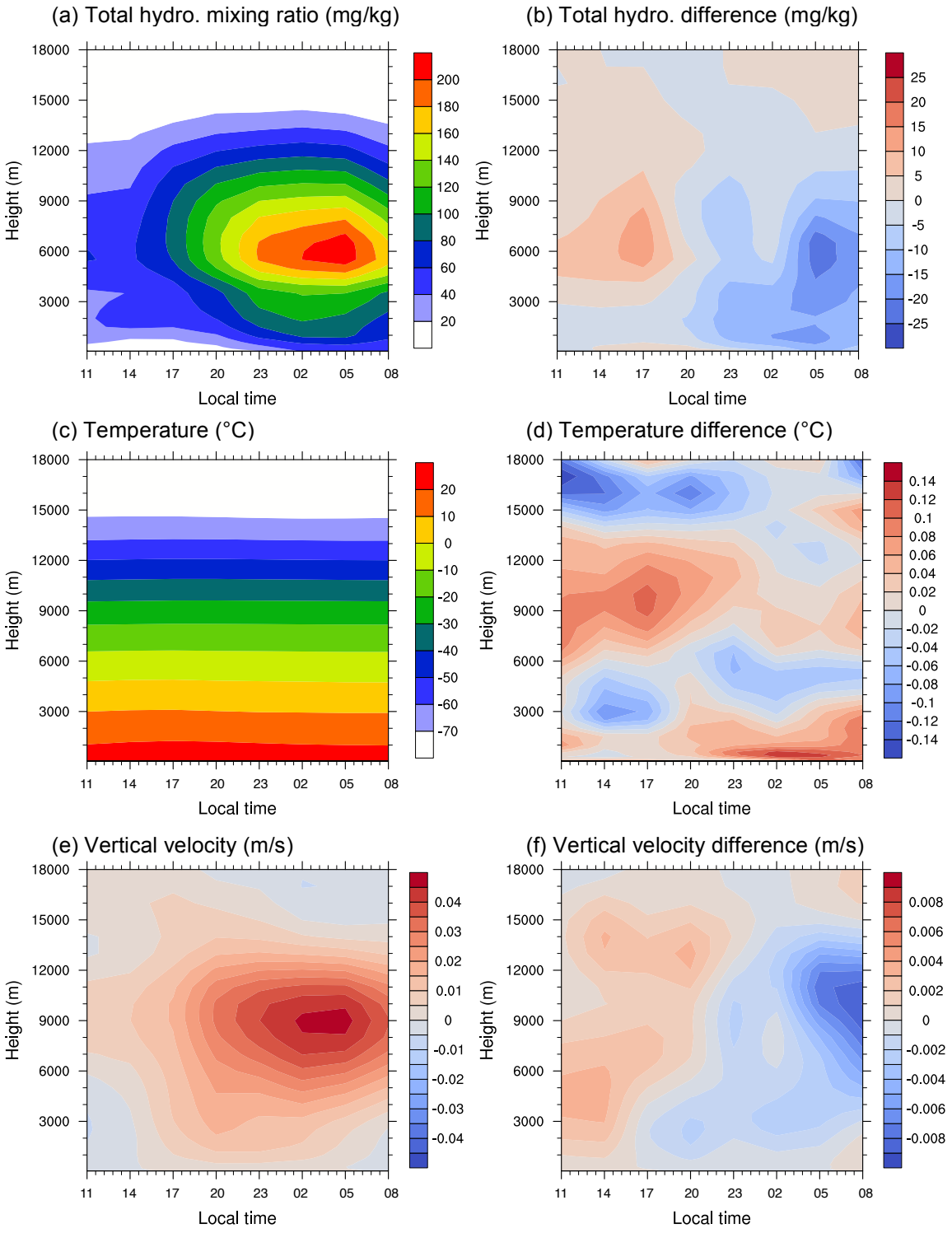

Figure 12. Diurnal evolution of vertical profiles over the Borneo region (r2) in FF for (a) total hydrometeor mixing ratio (mg kg^{-1}), (c) temperature (°C), and (e) vertical velocity (m s^{-1}). Data are averaged all the nocturnal convections. (b), (d), and (f) is the differences between FF and FFBB (FFBB-FF) for each parameter.

927

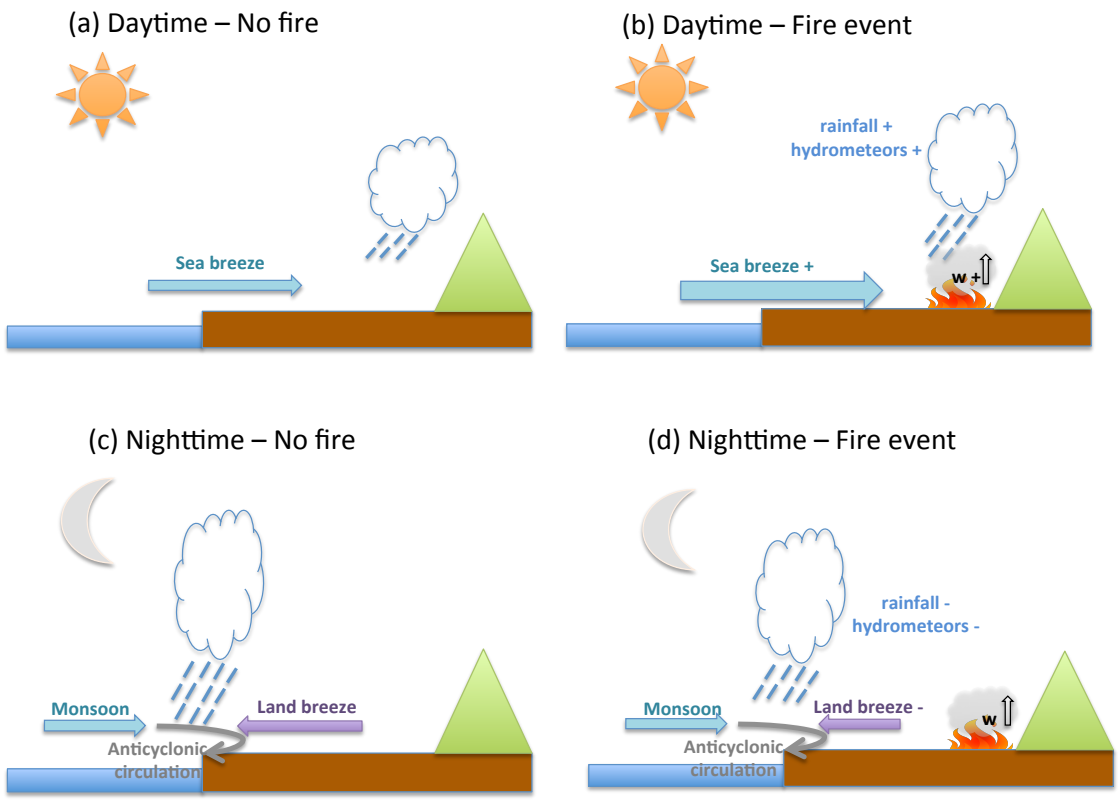

928

929 Figure 13. Schematics of diurnal rainfall/convection activity over the western Borneo. (a)
930 and (b) illustrate the formation of convection during the daytime without and with fire event,
931 respectively. (c) and (d) are the same as (a) and (b) but in the nighttime.

932